Materials Science in Semiconductor Processing 87 (2018) 126–133

Contents lists available at ScienceDirect

Materials Science in Semiconductor Processing

journal homepage: www.elsevier.com/locate/mssp

Ultrasonic-assisted hot pressing of Bi_2Te_3-based thermoelectric materials

Deqing Mei[a,b,*], Hui Wang[a,b], Zhehe Yao[c,**], Yang Li[b]

[a] State Key Laboratory of Fluid Power and Mechatronic Systems, School of Mechanical Engineering, Zhejiang University, Hangzhou 310027, China
[b] Key Laboratory of Advanced Manufacturing Technology of Zhejiang Province, School of Mechanical Engineering, Zhejiang University, Hangzhou 310027, China
[c] Institute of Laser Advanced Manufacturing, Zhejiang University of Technology, Hangzhou 310014, China

ARTICLE INFO

Keywords:
Bi_2Te_3
Ultrasonic-assisted hot pressing
Dynamic recrystallization
Thermoelectric property

ABSTRACT

In this study, *n*-type Bi_2Te_3-based bulk materials were prepared using the ultrasonic-assisted hot pressing. The effects of ultrasonic vibration on the mechanical and thermoelectric properties of the prepared samples were investigated. Field-emission scanning electron microscope (FESEM) tests revealed that the ultrasonic vibration refined the grain size to the submicron level. The grain size became smaller as the ultrasonic vibration duration is extended. The results showed that the sample with an ultrasonic vibration duration of 20 min (namely, Ultra 20) has a hardness of 64 HV0.3 and a flexural strength of 22.4 MPa, which represents an 82.9% and 50.2% improvement, respectively, over the untreated hot-pressed sample (namely, Ultra 0). As the ultrasonic vibration duration increased, the absolute value of the Seebeck coefficient was found to increase, whereas the electrical conductivity and the thermal conductivity decreased. The maximum dimensionless figure of merit (ZT_{max}) was 0.78 at 480 K for the Ultra 20 sample, which was 10.9% and 16.4% higher than the Ultra 10 and Ultra 0 samples, respectively. The results proved that both the mechanical properties and the thermoelectric properties of the $Bi_2Te_{2.7}Se_{0.3}$ bulk materials are improved by ultrasonic vibration.

1. Introduction

Bismuth telluride (Bi_2Te_3) and its alloys have been used as the predominant thermoelectric materials for applications near room temperature [1]. Continuous efforts have been made by the scholars around the world [2] to increase the figure of merit (*ZT*) value of the Bi_2Te_3-based bulk materials. On the other hand, the mechanical properties of the Bi_2Te_3-based bulk materials are also critical for the long-term reliability of the thermoelectric module. Simultaneously increasing both the thermoelectric and the mechanical properties of the Bi_2Te_3-based bulk materials will greatly promote the actual application of the materials.

There are numerous processes to fabricate the Bi_2Te_3-based bulk materials, which significantly affected their thermoelectric and mechanical properties [3,4]. Wang et al. [5] applied hot-deforming of powders to fabricate $Bi_2Te_{2.7}Se_{0.3}$ alloys with high thermoelectric performance, resulting in a flexural strength of 10 MPa. Zheng et al. [6] investigated the mechanical properties of p-type $Bi_{0.5}Sb_{1.5}Te_3$ commercial zone-melting (ZM) ingots, and the results showed that the flexural strength perpendicular to the ZM direction was 9.6 MPa. Shin et al. [7] fabricated $Bi_{0.5}Sb_{1.5}Te_3$ bulk materials with a flexural strength of 50.1 MPa by the hot-pressing of powders, with a maximum dimensionless figure of merit of 0.87 at room temperature. Ivanova et al. [8] combined hot-pressing with annealing in $Bi_{0.5}Sb_{1.5}Te_3$ solid solutions to remove imperfections in the structure. The compressive strength of the obtained material was 67 MPa while the annealing process tends to induce grain growth. Williams et al. [9] fabricated p-type $Bi_{0.5}Sb_{1.5}Te_3$ thermoelectric materials by spark plasma sintering using powder dispersed with nano-B_4C. The Vickers hardness was 80 HV0.3 in the direction perpendicular to solidification, while it dropped to 57 HV0.3 in the direction parallel to solidification.

Since the bismuth telluride crystals are easily cleaved perpendicular to the direction of the *c*-axis (basal plane) [10], the mechanical properties parallel to the crystal-growth direction were worse than those perpendicular to the crystal-growth direction for most of the studies mentioned above. Considering that ultrasonic vibration is able to refine grains and make the materials more isotropic [11–13], the mechanical properties of the materials can be improved by the ultrasonic vibration. Furthermore, finer grains contribute to a lower thermal conductivity [14,15], which potentially improve the thermoelectric properties of the materials. Appling ultrasonic vibration in hot pressing of Bi_2Te_3-based thermoelectric materials potentially improve both the mechanical and

* Corresponding author at: State Key Laboratory of Fluid Power and Mechatronic Systems, School of Mechanical Engineering, Zhejiang University, Hangzhou 310027, China.
** Corresponding author at: Institute of Laser Advanced Manufacturing, Zhejiang University of Technology, Hangzhou 310014, China.
E-mail addresses: meidq_127@zju.edu.cn (D. Mei), zhyao@zjut.edu.cn (Z. Yao).

https://doi.org/10.1016/j.mssp.2018.07.019
Received 12 December 2017; Received in revised form 6 June 2018; Accepted 10 July 2018
Available online 18 July 2018
1369-8001/

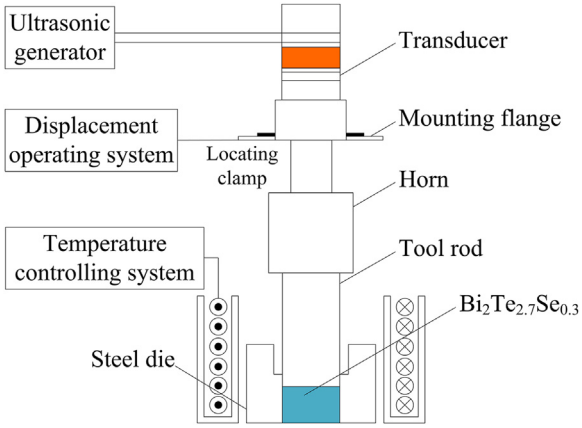

Fig. 1. Schematic diagram of the experimental setup for ultrasonic-assisted hot pressing.

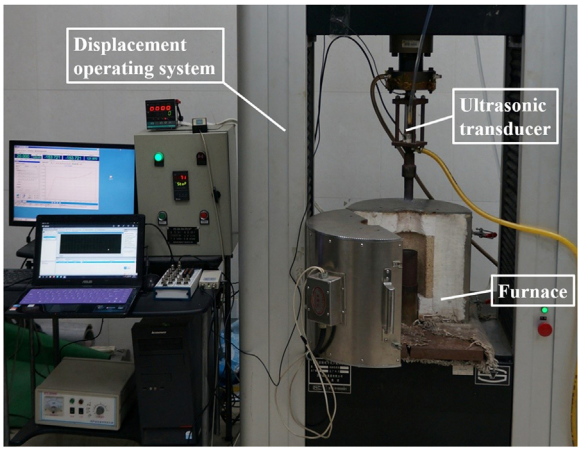

Fig. 2. Experimental setup for ultrasonic-assisted hot pressing.

the thermoelectric properties. To the authors' best knowledge, there is still no studies focusing on the ultrasonic-assisted hot pressing of bulk thermoelectric materials.

In this study, ultrasonic-assisted hot pressing was used to fabricate Bi_2Te_3-based alloys. The effects of ultrasonic vibration on the microstructures of the Bi_2Te_3-based alloys were investigated, along with its influence on the thermoelectric and the mechanical properties.

2. Experimental setup and procedures

An experimental setup was developed to apply the ultrasonic vibrations in the hot pressing process. The experimental setup consisted of an ultrasonic transducer, a horn, a tool rod, a heating furnace, and a die, as shown in Fig. 1. The transducer is made up of cylindrical piezoelectric elements, and its frequency and voltage can be adjusted continuously by the ultrasonic generator. The shape and the length of the horn are designed to have a longitudinal resonance frequency of 20 kHz. The displacement and the load are controlled by the displacement operating system (WDW-100E, Time Group Inc.). The furnace temperature is controlled by the temperature controlling system (GH-1, Yangzhou Guihao Inc.).

The *n*-type $Bi_2Te_{3-x}Se_x$ has proved to have excellent thermoelectric properties near room temperature. According to the previous reports [16], doping with Se element by x = 0.15–0.3 in $Bi_2Te_{3-x}Se_x$ system is able to obtain appropriate carrier concentrations to balance the electrical conductivity and the Seebeck coefficient, and thus optimize the power factor. Therefore, in this study, the *n*-type $Bi_2Te_{2.7}Se_{0.3}$ was selected and purchased from Leshan KaiYada Photoelectric Technology Co., Ltd. The as-received *n*-type $Bi_2Te_{2.7}Se_{0.3}$ ingots were made by the zone melting process, which is as follows. The constituent elements of Bi, Te, and Se with a purity of 99.9% were weighted in the stoichiometric proportions of $Bi_2Te_{2.7}Se_{0.3}$. The powder mixtures of elements were charged into a carbon-coated quartz tube that was sealed under 10^{-5} Torr. Bi, Te, and Se in the quartz tube were melted at 650 °C for 2 h using a rocking furnace to ensure composition homogeneity, and quenched to room temperature. The crystals were grown by the zone melting method using the temperature gradient of 25 °C/mm and growth rate of 8 mm/h.

The as-received *n*-type $Bi_2Te_{2.7}Se_{0.3}$ ingot was loaded into a high-speed vibratory ball mill (SFM-3, Hefei Ke Jing Materials Technology Co., LTD, China), and was pulverized for 2 h into fine powder at a speed of 1200 rpm without the protection of inert atmosphere. The ball-to-powder weight was 20:1. Before hot pressing, the powders were cold compacted under 60 MPa without evacuation to densify the powders at room temperature. The cold compacting was conducted in a steel die with an internal diameter of 12.7 mm. The cold-compacted powders were then hot-pressed at 823 K under a uniaxial pressure of 60 MPa for 20 min. Ultrasonic vibration generated by the ultrasonic transducer with a frequency of 20 kHz and amplitude of 26 μm was applied from the beginning of the hot pressing process to influence the material microstructures, as shown in Fig. 2. To study the effect of ultrasonic vibration duration on the materials, the samples were applied with vibration durations of 0, 10, and 20 min, respectively. After hot-pressing with various ultrasonic vibration durations, the samples were furnace cooled to room temperature. The as-achieved $Bi_2Te_{2.7}Se_{0.3}$ bulk samples were then named Ultra 0, Ultra 10, and Ultra 20, respectively.

The phase identification of the samples were performed by X-ray diffraction (XRD, PANalytical X'pert PRO with a Cu K_α radiation, wavelength = 1.54 Å). The chemical composition measurements of the *n*-type $Bi_2Te_{2.7}Se_{0.3}$ bulk sample after consolidation were performed by energy-dispersive X-ray spectroscopy (EDS, Hitachi S-3700N, Hitachi, Japan). The flexural strength of the bulk material was tested using a three-point flexural method as shown in Fig. 3. The flexural test was conducted on a three-axis linear stage (Newport 460 P, Irvine, CA, USA) and the three-point flexural test was carried out using a rectangular bar with the dimension of 11 mm × 3 mm × 2 mm. The flexural strength (σ_f) was calculated using the equation $\sigma_f = 3PL/2bh^2$, where P is the measured peak load at failure, L is the span length, and b and h are the width and thickness of the sample, respectively. The span length for three-point flexural test was 6 mm. The load was measured using a force sensor (Interface 3A120, USA) with a resolution of 0.01 N. At least 5 samples were used for the flexural strength test for Ultra 0, Ultra 10, and Ultra 20, respectively. The Vickers hardness tests were performed with a Vickers microhardness tester (MH-5, Everone, China). A load of 2.94 N (0.3 kgf) was applied for 10 s using a square-base diamond pyramid. Five indentations were performed on each sample and the average of five samples was used to evaluate the Vickers hardness value for Ultra 0, Ultra 10, and Ultra 20 samples, respectively. The morphologies of the bulk samples were analyzed by field-emission scanning electron microscopy (FESEM, FEI Sirion100, USA). Disk samples (Φ12.7 mm × 2 mm) were prepared for measurement of the thermal conductivity κ. Rectangular samples (3 mm × 2 mm × 10 mm) were prepared for measurement of the electrical conductivity σ and the Seebeck coefficient α. The specific heat C_p was measured using a Netzsch DSC 404C (Netzsch, Selb, Germany), and the thermal diffusivity λ was measured using a Netzsch LFA 457 (Netzsch, Selb, Germany). The sample density ρ was measured by the Archimedes method. The thermal conductivity κ was then calculated using the formula: $\kappa = \lambda\rho C_p$. The electrical conductivity σ and the Seebeck coefficient α were simultaneously measured when a temperature difference was applied between two ends of the sample, using a commercial Linseis® LSR-3 system (Linseis, Germany). The Hall coefficient R_H of the sample was measured at 298 K on a Quantum Design PPMS-9T instrument using a four-probe configuration, with the magnetic field sweeping

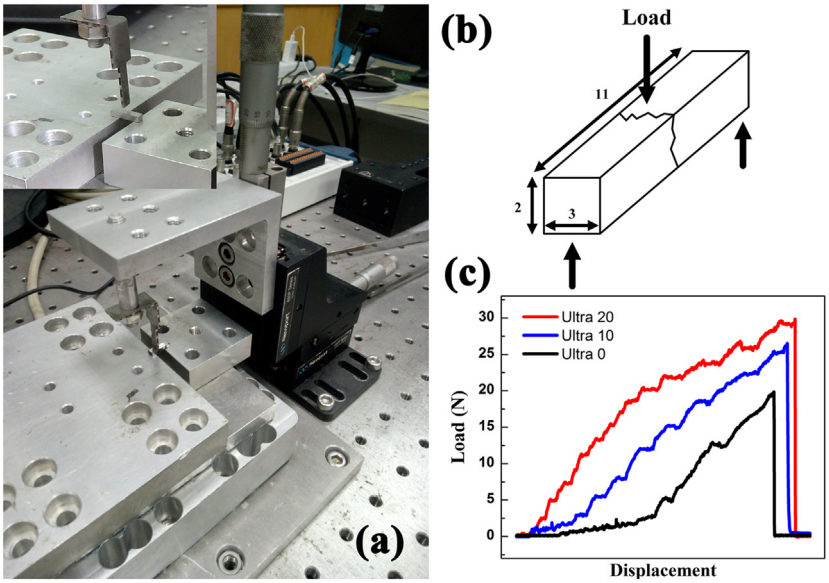

Fig. 3. The flexural strength testing: (a) three-axis linear stage, (b) illustration of the three-point flexural test method, (c) load-displacement curves of the hot-pressed samples with various ultrasonic vibration durations.

between ± 4.0 T. The electrical current I was fixed at 100 mA. Rectangular samples with the dimension of 0.2 × 2 × 10 mm^3 were used for the test. The formula $R_H = V_H d/IB$ was used to calculate the Hall coefficient, where V_H is the measured Hall voltage, d is the thickness of the sample, I is the electrical current and B is the magnetic field intensity. The slope of V_H versus B was used to avoid the inherent deviation. 17 data points of V_H and B were used to calculate the Hall coefficient R_H. The carrier concentration n and the mobility μ were calculated according to $n = 1/R_H e$ and $\sigma = ne\mu$, where e is the electron charge.

3. Experimental results

3.1. The effects of ultrasonic vibration on the microstructures

The transformation of the microstructure of the bulk samples are investigated by FESEM. The fracture FESEM micrographs of the samples sintered under 823 K with the ultrasonic vibration of 0 min, 10 min, and 20 min are shown in Fig. 4**(a)**, **(b)**, and **(c)**, respectively. For all the bulk samples, the grains were found to be randomly oriented. Although partially oriented lamellar structure can be observed at some regions, there are no obvious large-scale preferred orientations in these bulk samples. The fracture morphology of the n-type $Bi_2Te_{2.7}Se_{0.3}$ bulk samples treated with ultrasonic vibration are similar to the untreated samples, except for the refined grain sizes. It can be noted that the grain sizes decreased as the ultrasonic vibration duration increased. The line interception method was used to calculate the grain size of the bulk samples. Five lines are drawn across the SEM photographs with the same spacing. Three samples were prepared for each experimental setting, and the SEM photographs from three different fracture surfaces for each sample were used in the calculation. The drawing and the calculation process are conducted by software “Nano Measurer”, and the results are summarized in Table 1. The average grain size of the Ultra 0, Ultra 10, and Ultra 20 bulk samples was 2.82 μm, 1.45 μm, and 1.11 μm, respectively. When the grain size is reduced, the scattering of the charge carriers and the phonons are strengthened due to the increased grain boundary area. The carriers are less scattered than the phonons due to their mean free path (MFP) of several nanometers. As the phonons with a mean free path of 800 nm ~ 1 μm nearly accumulate around 20% of the lattice thermal conductivity at room temperature, the grain size under 1 μm has a significant effect in reducing the lattice thermal conductivity. As shown in Fig. 4**(c)** and Table 1, because of the ultrasonic vibration, the grains with a size of 800 nm ~ 1 μm exist extensively in the Ultra 20 sample, implying an enhanced long-MFP phonon scattering in the Ultra 20 sample.

Phase identification was performed to further study the effect of the ultrasonic vibration on phase structures of the bulk materials. The XRD patterns of the ball-milled powders and the $Bi_2Te_{2.7}Se_{0.3}$ bulk samples under various ultrasonic vibration durations are shown in Fig. 5. Compared with the ball-milling powders, the XRD peaks of sintered alloys become shaper and stronger after the powders were hot-pressed, as seen in the 006 and the 1010 peaks, indicating the improvement in crystallinity and the release of crystalline defects and remnant stress in the powders after the hot-pressing process. The ultrasonic vibration has not changed the phase structure of the $Bi_2Te_{2.7}Se_{0.3}$ material.

3.2. The effects of ultrasonic vibration on the thermoelectric properties

The temperature dependences of the thermoelectric properties of the bulk samples under various ultrasonic vibration durations are shown in Fig. 6. The error bars show that the errors in the measurements were ≤ 5% for α and κ, and ~ 7% for σ. As shown in Fig. 6**(a)**, the electrical conductivity (σ) decreases monotonically with increasing the ultrasonic vibration duration. From Fig. 6**(b)**, the negative value of the Seebeck coefficients shows that all the samples are n-type semiconductors. The absolute values of the Seebeck coefficients of the samples increase as the ultrasonic vibration duration increases. The absolute value of the maximum Seebeck coefficient increased from 147 μV/K to 149.4 μV/K, and further increased to 156 μV/K, for the Ultra 0, Ultra 10, and Ultra 20 samples, respectively. A total enhancement of 6% is achieved after the bulk sample was ultrasonic treated for 20 min compared with the untreated hot-pressed sample. Because the Seebeck coefficient is always inversely proportional to the carrier concentration (n), as [17]

$$S = 8\pi^2\kappa_B^2 Tm^*(\pi/3n)^{2/3}/3eh^2, \quad (1)$$

where κ_B, e, h and m^* are the Boltzmann constant, the elementary charge, the Planck constant and the density of states effective mass, respectively, the variation of the Seebeck coefficient shows an opposite tendency with respect to electrical conductivity, as shown in Fig. 6**(a)** and **(b)**.

The temperature dependence of the power factor ($PF = \alpha^2\sigma$)

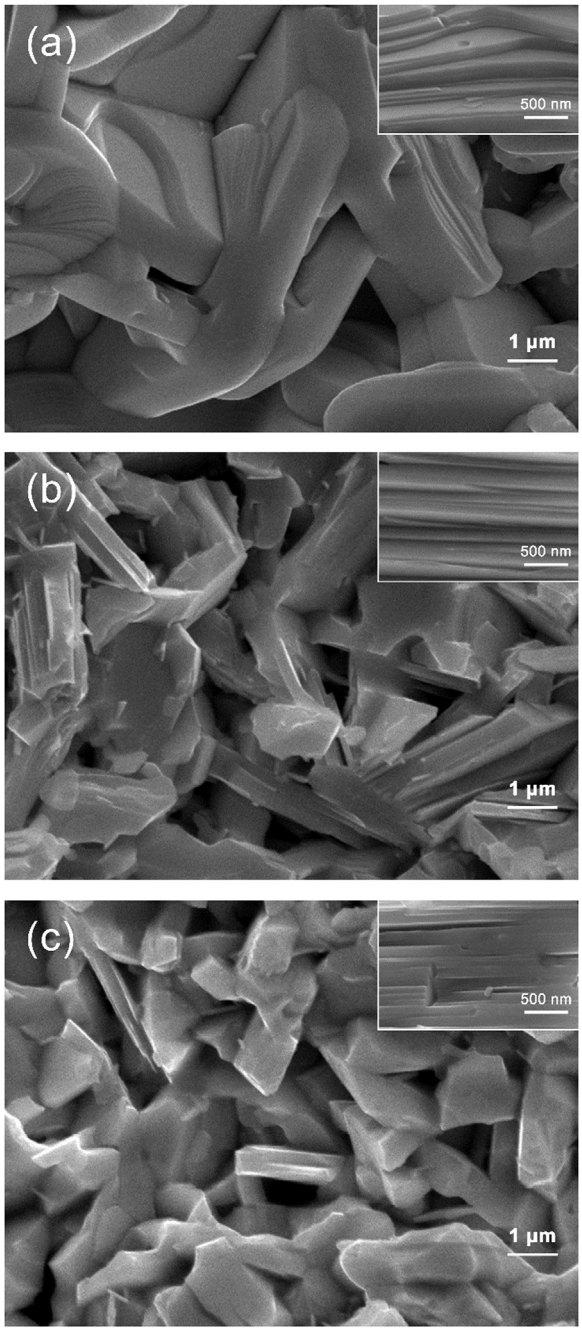

Fig. 4. FESEM micrographs of $Bi_2Te_{2.7}Se_{0.3}$ bulk samples: (a) without ultrasonic vibration, (b) with 10-min ultrasonic vibration, (c) with 20-min ultrasonic vibration. The insets indicate the lamellar structure from the zone-melting method with high resolution.

Table 1
Statistical results of the grain sizes of the hot-pressed samples with various ultrasonic vibration durations.

Samples	Average grain size	Grain size distribution	Primary grain size distribution and its percentage	
Ultra 0	2.82 μm	1.33–4.9 μm	3–3.4 μm	21.74%
Ultra 10	1.45 μm	0.43–3.23 μm	1.2–1.6 μm	30.23%
Ultra 20	1.11 μm	0.4–3.64 μm	0.8–1.2 μm	36.84%

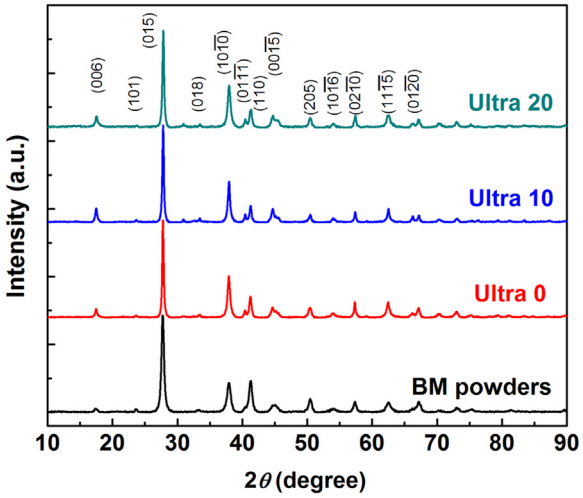

Fig. 5. XRD patterns of the $Bi_2Te_{2.7}Se_{0.3}$ ball-milling (BM) powders and the hot-pressed samples under various ultrasonic vibration durations.

calculated from the Seebeck coefficient and the electrical conductivity data is plotted in Fig. 6**(c)**. The hot-pressed sample shows a power factor of 1.10×10^{-3} W m^{-1} K^{-2} at 500 K. When the ultrasonic vibration duration increased, the value of the power factor shows a slight increase. A maximum power factor of 1.15×10^{-3} W m^{-1} K^{-2} and 1.22×10^{-3} W m^{-1} K^{-2} at 480 K is obtained by the Ultra 10 and Ultra 20 samples, respectively, which mainly results from the higher Seebeck coefficients of the samples.

For thermoelectric materials, the total thermal conductivity is composed of the electronic thermal conductivity (κ_e) and the lattice thermal conductivity (κ_l): $\kappa = \kappa_e + \kappa_l$. The electronic thermal conductivity κ_e can be estimated from the Wiedemann-Franz law as $\kappa_e = L\sigma T$, where L is the Lorenz constant which can be taken as 2.45×10^{-8} W Ω K^{-2} for a degenerate semiconductor, σ is the electric conductivity, and T is the absolute temperature. Thus, lattice thermal conductivity κ_l could be obtained by subtracting κ_e from κ. The temperature dependence of the total thermal conductivity κ and the lattice thermal conductivity κ_l are shown in Fig. 6**(d)** and Fig. 6**(e)**, respectively.

From Fig. 6(d), the thermal conductivity (κ) of the samples decreased with an increased measurement temperature, and the minimum values of the thermal conductivity for the Ultra 0, Ultra 10, and Ultra 20 samples reached 0.79, 0.76, and 0.72 W m^{-1} K^{-1}, respectively, at ~ 380 K. When the temperature is higher than 380 K, the intrinsic excitation increases the carrier concentration, and the increased bipolar thermal conductivity has contributed to an increase of the κ. From Fig. 6(e), the minimum lattice thermal conductivity κ_l of the Ultra 0, Ultra 10, and Ultra 20 samples are reduced from ~ 0.20 to 0.17, and further to 0.15 W m^{-1} K^{-1}. The decrease of κ_l has led to the decrease of the total thermal conductivity κ.

Fig. 6**(f)** shows the temperature dependence of the dimensionless figure of merits of the bulk samples. The maximum ZT values of the bulk samples can be achieved at the temperature range from 480 K to 500 K. For the Ultra 0 sample, a maximum ZT value of 0.67 is achieved at 500 K. For the Ultra 10 sample, the maximum ZT value of 0.71 can be reached at 500 K, which corresponds to a 6% enhancement as compared to the Ultra 0 sample. The maximum ZT value of the Ultra 20 sample reaches 0.78 at around 480 K. The increase results from its higher power factor and lower total thermal conductivity. The ZT value of the Ultra 20 sample has shown a 16.4% enhancement as compared to the Ultra 0 sample, as shown in Fig. 6**(f)**.

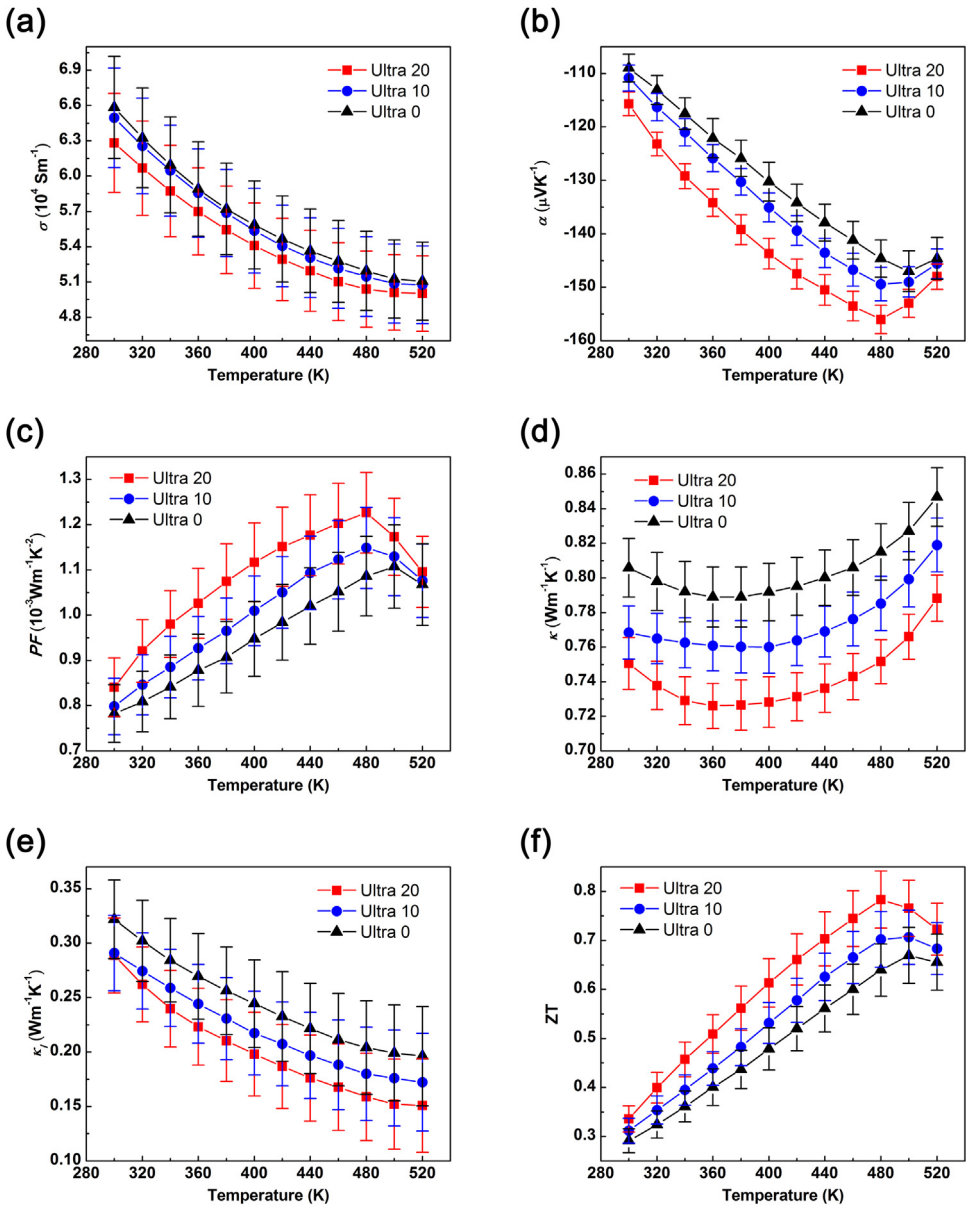

Fig. 6. Temperature dependence of (a) electrical conductivity σ, (b) Seebeck coefficient α, (c) power factor $\alpha^2\sigma$, (d) total thermal conductivity κ, (e) lattice thermal conductivity κ_l, and (f) dimensionless figure of merit ZT of the hot-pressed samples with various ultrasonic vibration durations.

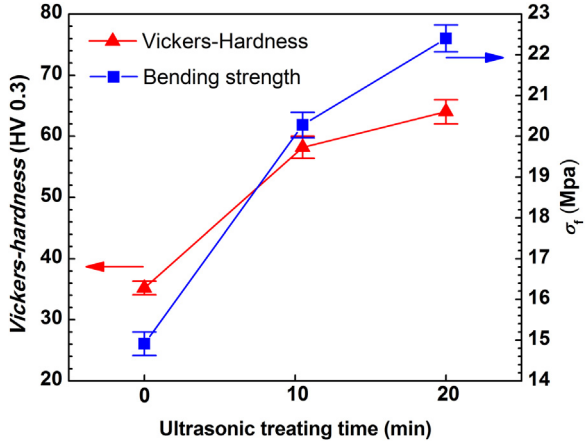

Fig. 7. Mechanical properties of the hot-pressed $Bi_2Te_{2.7}Se_{0.3}$ bulk samples with various ultrasonic vibration durations.

3.3. The effects of ultrasonic vibration on the mechanical properties

The mechanical properties of the bulk samples are shown in Fig. 7 and the statistical results are shown in Table 2. The Vickers hardness values and the flexural strength σ_f both increased as the ultrasonic vibration duration increased. The average value of the Vickers hardness reached 35.2, 58.2, and 64 HV0.3, respectively, for the Ultra 0, Ultra 10, and Ultra 20 samples. According to the Hall-Petch equation, the hardness of the material will increase when the grain size decreased [18]. The Ultra 20 sample and the Ultra 10 sample have smaller grain size than the Ultra 0 sample. The reduced grain size has resulted in an increased hardness value in these ultrasonic-treated samples. This increase can be finally attributed to the increased grain boundaries, which act as strong obstacles to the dislocation motion. The average flexural strength of the bulk samples were 14.9 MPa, 20.3 MPa and 22.4 MPa, respectively, for the Ultra 0, Ultra 10, and Ultra 20 samples. The improvement in flexural strength should also be attributed to the grain size refinement after ultrasonic vibration. According to Pan's study [19], for Bi_2Te_3-based materials, the mechanical strength

Table 2
Statistical results of the flexural strength and Vickers hardness of the hot-pressed samples with various ultrasonic vibration durations.

Samples	Number of samples	Flexural strength (MPa)	Standard deviation (MPa)	Number of samples/indentations	Vickers hardness (HV0.3)	Standard deviation
Ultra 0	5	14.91	0.29	5/25	35.23	1.11
Ultra 10	5	20.30	0.31	5/25	58.21	1.81
Ultra 20	6	22.39	0.33	5/25	64.02	1.96

increases when the grain size decreases. The increased grain boundary area inhibits the crack propagation, which benefits the flexural strength.

4. Discussion

In the present study, the effects of superimposed ultrasonic vibration on the thermoelectric properties and the mechanical properties are not solely derived from one mechanism. The high-frequency vibration and shock applied on the samples in elevated temperatures may break and refine the grains. Furthermore, the ultrasonic vibration energy is not absorbed uniformly throughout the material, but is mostly absorbed by dislocations, grain boundaries, etc. Ultrasonic waves caused by the ultrasonic vibrations can be scattered or absorbed at the nonuniform portions, then the amplitude of the dislocation vibration will approach its balance position, resulting in the decrease of the activation energy. The reduction of the activation energy leads to the increase of both the dislocation density and average velocity of the mobile dislocations. The increased mobile dislocations with a higher average velocity are considered to promote the subgrain formation [20–23]. Then, the dynamic recrystallization including the grain refinement and the dislocation rearrangement due to the ultrasonic vibration significantly affect the thermoelectric properties and the mechanical properties. In addition, applying ultrasonic vibration in hot pressing of thermoelectric materials may enhance the bonding force, resulting in improvement of the mechanical properties. Previous studies [24–27] indicated that the ultrasonic energy is mostly absorbed by the dislocations and grain boundaries. Extending the ultrasonic duration also proved beneficial to the dislocation generation [28].

In the present study, the hot-pressing process and ultrasonic vibration were conducted simultaneously. After the temperature was elevated, the dislocations disappeared and the distortion energy within deformed samples was released. New submicron grains were created as the dislocations disappeared. In this process, both the dislocation multiplication and elimination, namely “dynamic recrystallization [29,30]” occurs. According to Chen's theory [31], the dynamic recrystallization process can be described as high dislocation density → dislocation network → subgrain → dynamic recrystallization grain. It is regarded that dynamic recrystallization process in the ultrasonic-assisted hot pressing resulted in refinement of the grains in the $Bi_2Te_{2.7}Se_{0.3}$ bulk samples.

It is noteworthy from Fig. 5 that all the characteristic peaks of the bulk samples were only indexed as $Bi_2Te_{2.7}Se_{0.3}$ phase with a rhombohedral lattice structure (space group of *Rm*) as reported previously [32,33], indicating that the ultrasonic vibration has not changed the phase structure of the $Bi_2Te_{2.7}Se_{0.3}$ material. It should be also noted from Fig. 5 that for all the $Bi_2Te_{2.7}Se_{0.3}$ bulk samples, no obvious enhancements in the intensity of *00 l* peaks have taken place, which is consistent with the FESEM results, as is shown in Fig. 4.

There is little variation of Seebeck coefficients as seen in Fig. 6**(b)**. The Seebeck coefficient can be affected by the grain-boundary carrier-filtering effect and the variation of the carrier concentration *n*. For further investigation, the room-temperature carrier concentration (*n*) and mobility (μ) of the bulk samples with various ultrasonic vibration durations were measured and are shown in Table 3. In the Hall coefficient measurement, all the 17 data points showed a good linearity. A theoretical calculation based on the Boltzmann transport equation is

Table 3
Room-temperature carrier concentration (*n*), mobility (μ), and Hall coefficient (R_H) of the hot-pressed samples with various ultrasonic vibration durations.

Samples	Carrier concentration (*n*) $\times 10^{19}$ (cm^{-3})	Carrier mobility μ (cm^2/Vs)	Hall coefficient R_H ($cm^3\ C^{-1}$)
Ultra 20	8.05	48.7	− 0.0776
Ultra 10	8.16	49.7	− 0.0766
Ultra 0	8.18	50.3	− 0.0764

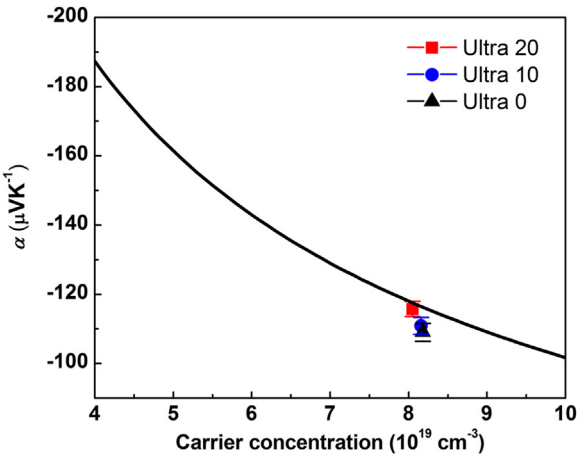

Fig. 8. Seebeck coefficient (α) as a function of the carrier concentration (*n*) at room temperature for the $Bi_2Te_{2.7}Se_{0.3}$ bulk materials. The symbols indicate the room-temperature Seebeck coefficient of the hot-pressed bulk samples with various ultrasonic vibration durations.

performed to plot the Pisarenko relation (i.e. carrier concentration vs. Seebeck coefficient), as shown in Fig. 8. The calculation is under the assumption that $m^*/m_e = 1.09$, where m^* is the density of state (DOS) effective mass, and m_e is the free electron mass [34]. There are very small deviations between the experimentally measured Seebeck coefficients and the numerically calculated values, and no significant enhancement of the Seebeck coefficient was found from Pisarenko plots. This implies that the grain boundaries did not play a significant role in the carrier energy filtering effect. The variation of the Seebeck coefficient of the Ultra 0, Ultra 10 and Ultra 20 samples should be attributed to the change of the carrier concentration. The electrical conductivity (σ) slightly decreases when the ultrasonic vibration duration increases, as shown in Fig. 6**(a)**. This trend could be resulted from the variation of the carrier concentration (*n*) and mobility (μ) with increasing ultrasonic vibration duration. When extending the ultrasonic vibration duration, the reduced grain sizes only slightly affected the carrier scattering, leading to a small change of the room-temperature μ from 50.3 cm^2/Vs, to 49.7 cm^2/Vs, to 48.7 cm^2/Vs. The reduction of the carrier mobility is caused by the increased grain boundaries, where the grain boundaries impede the conduction of the carriers between grains. When the ultrasonic vibration duration was extended, the room-temperature carrier concentration (*n*) decreased gradually from 8.18×10^{19} cm^{-3}, to 8.16×10^{19} cm^{-3}, and further decreased to 8.05×10^{19} cm^{-3}. In the prior ball-milling process, vacancies like the tellurium vacancies V_{Te} and the selenium vacancies V_{Se} were introduced, which act as

Table 4
EDS results of the chemical composition of the n-type $Bi_2Te_{2.7}Se_{0.3}$ bulk sample after consolidation.

Element/composition Atom (%)	Ultra 0	Ultra 10	Ultra 20
Bi	41.67 ± 2.97	42.48 ± 3.02	41.99 ± 2.92
Te	54.42 ± 3.42	53.63 ± 3.90	54.06 ± 3.86
Se	3.91 ± 0.13	3.89 ± 0.14	3.95 ± 0.14
Composition	$Bi_{2.08}Te_{2.72}Se_{0.195}$	$Bi_{2.12}Te_{2.68}Se_{0.195}$	$Bi_{2.1}Te_{2.7}Se_{0.198}$

contributors of the electron carrier concentrations in the $Bi_2Te_{2.7}Se_{0.3}$ bulk materials [32,33]. This slight change of the carrier concentration may be attributed to the reduction of V_{Te} and V_{Se} during the dynamic recrystallization process. The chemical composition of the samples after consolidation measured by EDS is also listed in Table 4. Slight evaporation of Se and Te are found in bulk samples after consolidation. The Se and Te evaporation could increase the electrical conductivity of the bulk samples by increasing the carrier concentrations.

It is considered that the reduction of κ_l for the Ultra 10 and Ultra 20 samples is mainly due to the enhanced phonon scattering at the grain boundaries with refined grain sizes. The mean free path (MFP) of phonons were estimated using the full distribution of MFPs. Under this assumption, phonons with the MFPs from few nanometers to hundreds of micrometers all contribute to the lattice thermal conductivity. And the phonons scattered at the grain boundaries were calculated according to the BvK model [35]:

$$L_{boundary} = \alpha_B D_{ave}, \tag{2}$$

where L_{boundary} is the MFP of the phonon scattered at the grain boundary, α_B, accounting for the effect of grain boundary transmission, is taken as 0.86 according to the Bvk model, and D_{ave} is the average grain size of the sample.

Combined with Eq. (2), the model established by Dames and Chen [36] is used to evaluate the effect of the grain size on the lattice thermal conductivities. According to the Dames model, the phonon MFP-dependent contributions to lattice thermal conductivity can be expressed as

$$k_{accum}(\omega) = \Sigma \int_0^{\infty} \frac{1}{3} C(\omega) v(\omega) L(\omega) d\omega, \tag{3}$$

where ω is the phonon frequency, C is the specific heat per unit phonon frequency, v is the group velocity, and L is the phonon MFP. Based on the model's prediction results, phonons with an MFP of less than 1 μm are the major components of the lattice thermal conductivity for the Bi_2Te_3-based bulk materials [36–38]. In the present work, the lamellar structure of the bulk materials has strongly blocked the phonons with high frequency, which leads to the largest reduction of the lattice thermal conductivity κ_l. However, the refined grains of the ultrasonic-treated samples has mainly scattered the phonons with a MFP from a few hundred nanometers to a few microns, leading to a further reduction of the lattice thermal conductivity κ_l.

Due to the highly anisotropic thermoelectric properties of the p-type Bi_2Te_3 materials, the thermoelectric performance perpendicular to the pressing direction is much higher than that parallel to the pressing direction. Simply reducing the grain size by the ultrasonic-assisted hot pressing is not necessarily useful in improving the thermoelectric properties in p-type Bi_2Te_3 materials.

5. Conclusion

Ultrasonic-assisted hot pressing was used to enhance the mechanical and thermoelectric properties of *n*-type $Bi_2Te_{2.7}Se_{0.3}$ bulk materials simultaneously. The ultrasonic vibration can obtain the final grain size with submicron by adjusting the vibration duration properly. The mechanical properties of the $Bi_2Te_{2.7}Se_{0.3}$ bulk materials were enhanced after ultrasonic vibration due to the refinement of the grain size. The average Vickers hardness of 64 HV0.3 and flexural strength of 22.4 MPa were obtained for the sample with 20 min of ultrasonic vibration, which corresponds to an 82.9% and 50.2% enhancement as compared to the untreated sample, respectively. The refined grains also enhanced the scattering of phonons by increasing the density of the grain boundaries, and reducing the lattice thermal conductivity κ_l. The maximum ZT value was 0.78 at 480 K for the Ultra 20 sample, which showed a 16.4% enhancement as compared to the Ultra 0 sample. The present study indicates that the ultrasonic-assisted hot-pressing is able to improve the mechanical and thermoelectric properties of *n*-type Bi_2Te_3-based materials.

Acknowledgements

The work was supported by the National Natural Science Foundation of China [Grant No. 51575482], Science Fund for Creative Research Groups of National Natural Science Foundation of China [Grant No. 51521064], and the Zhejiang Provincial Funds for Distinguished Young Scientists of China [Grant No. LR14E050002].

References

[1] P. Zou, G. Xu, S. Wang, Enhanced thermoelectric performance in n-type $Bi_2Te_{2.95}Se_{0.05}$ bulks fabricated by high pressure sintering technique, Mater. Res. Bull. 60 (2014) 808–813.
[2] L. Hu, T. Zhu, X. Liu, X. Zhao, Point defect engineering of high-performance Bismuth-Telluride-based thermoelectric materials, Adv. Funct. Mater. 24 (2014) 5211–5218.
[3] J.G. Park, Y.H. Lee, High thermoelectric performance of Bi-Te alloy: defect engineering strategy, Curr. Appl. Phys. 16 (2016) 1202–1215.
[4] M.K. Keshavarz, D. Vasilevskiy, R.A. Masut, S. Turenne, Mechanical properties of bismuth telluride based alloys with embedded MoS_2 nano-particles, Mater. Des. 103 (2016) 114–121.
[5] M. Wang, Z. Tang, T. Zhu, X. Zhao, The effect of texture degree on the anisotropic thermoelectric properties of $(Bi,Sb)_2(Te,Se)_3$ based solid solutions, RSC Adv. 6 (2016) 98646–98651.
[6] Y. Zheng, H. Xie, S. Shu, Y. Yan, H. Li, X. Tang, High-temperature mechanical and thermoelectric properties of p-Type $Bi_{0.5}Sb_{1.5}Te_3$ commercial zone melting ingots, J. Electron. Mater. 43 (2014) 2017–2022.
[7] H.S. Shin, H.P. Ha, D.B. Hyun, J.D. Shim, D.H. Lee, Thermoelectric properties of 25% Bi_2Te_3-75% Sb_2Te_3 solid solution prepared by hot-pressing method, J. Phys. Chem. Solids 58 (1997) 671–678.
[8] L. Ivanova, L. Petrova, Y.V. Granatkina, V. Leontyev, A. Ivanov, S. Varlamov, Y.P. Prilepo, A. Sychev, A. Chuiko, I. Bashkov, Thermoelectric and mechanical properties of the $Bi_{0.5}Sb_{1.5}Te_3$ solid solution prepared by melt spinning, Inorg. Mater. 49 (2013) 120–126.
[9] H.R. Williams, R.M. Ambrosi, K. Chen, U. Friedman, H. Ning, M. Reece, M. Robbins, K. Simpson, K. Stephenson, Spark plasma sintered bismuth telluride-based thermoelectric materials incorporating dispersed boron carbide, J. Alloy. Compd. 626 (2015) 368–374.
[10] P. Puneet, R. Podila, M. Karakaya, S. Zhu, J. He, T.M. Tritt, M.S. Dresselhaus, A.M. Rao, Preferential scattering by interfacial charged defects for enhanced thermoelectric performance in few-layered n-type Bi_2Te_3, Sci. Rep. 3 (2013).
[11] F. Djavanroodi, H. Ahmadian, R. Naseri, K. Koohkan, M. Ebrahimi, Experimental investigation of ultrasonic assisted equal channel angular pressing process, Arch. Civ. Mech. Eng. 16 (2016) 249–255.
[12] Y. Liu, S. Suslov, Q. Han, C. Xu, L. Hua, Microstructure of the pure copper produced by upsetting with ultrasonic vibration, Mater. Lett. 67 (2012) 52–55.
[13] V. Abramov, O. Abramov, B. Straumal, W. Gust, Hypereutectic Al-Si based alloys with a thixotropic microstructure produced by ultrasonic treatment, Mater. Des. 18 (1997) 323–326.
[14] L. Hu, H. Wu, T. Zhu, C. Fu, J. He, P. Ying, X. Zhao, Tuning multiscale microstructures to enhance thermoelectric performance of n-type Bismuth-Telluride-based solid solutions, Adv. Energy Mater. 5 (2015), https://doi.org/10.1002/aenm.201500411.
[15] M. Tan, Y. Deng, Y. Wang, Ordered structure and high thermoelectric properties of $Bi_2(Te,Se)_3$ nanowire array, Nano Energy 3 (2014) 144–151.
[16] C. Kim, C.E. Kim, J.Y. Baek, D.H. Kim, J.T. Kim, J.H. Ahn, D.H. Lopez, H. Kim, A novel chemical process of $Bi_2Te_{2.7}Se_{0.3}$ nanocompound for effective adjustment in transport properties resulting in remarkable n-type thermoelectric performance, Scr. Mater. 119 (2016) 13–16.
[17] M. Cutler, J. Leavy, R. Fitzpatrick, Electronic transport in semimetallic cerium sulfide, Phys. Rev. A 133 (1964) 1143.
[18] J. Jiang, Y. Wang, J. Qu, Microstructure and mechanical properties of AZ61 alloys with large cross-sectional size fabricated by multi-pass ECAP, Mater. Sci. Eng. A 560 (2013) 473–480.
[19] Y. Pan, T.-R. Wei, Q. Cao, J.-F. Li, Mechanically enhanced p-and n-type Bi_2Te_3-based thermoelectric materials reprocessed from commercial ingots by ball milling

and spark plasma sintering, Mater. Sci. Eng. 197 (2015) 75–81.
[20] X. Ye, T. Liu, Y. Ye, H. Wang, G. Tang, G. Song, Enhanced grain refinement and microhardness of Ti-Al-V alloy by electropulsing ultrasonic shock, J. Alloy. Compd. 621 (2015) 66–70.
[21] L. Shi, C.S. Wu, S. Gao, G.K. Padhy, Modified constitutive equation for use in modeling the ultrasonic vibration enhanced friction stir welding process, Scr. Mater. 119 (2016) 21–26.
[22] O. Izumi, K. Oyama, Y. Suzuki, Effects of superimposed ultrasonic vibration on compressive deformation of metals, Trans. Jpn. Inst. Met. 7 (1966) 162–167.
[23] Y. Liu, S. Suslov, Q. Han, C. Xu, L. Hua, Microstructure of the pure copper produced by upsetting with ultrasonic vibration, Mater. Lett. 67 (2012) 52–55.
[24] H. Zhou, H. Cui, Q.-H. Qin, H. Wang, Y. Shen, A comparative study of mechanical and microstructural characteristics of aluminium and titanium undergoing ultrasonic assisted compression testing, Mater. Sci. Eng. A 682 (2017) 376–388.
[25] Z. Liu, H. Fecht, M. Umemoto, Microstructural evolution and nanocrystal formation during deformation of Fe-C alloys, Mater. Sci. Eng. A 375 (2004) 839–843.
[26] Z. Yao, G.-Y. Kim, Z. Wang, L. Faidley, Q. Zou, D. Mei, Z. Chen, Acoustic softening and residual hardening in aluminum: modeling and experiments, Int. J. Plast. 39 (2012) 75–87.
[27] Z. Yao, G.-Y. Kim, L. Faidley, Q. Zou, D. Mei, Z. Chen, Effects of superimposed high-frequency vibration on deformation of aluminum in micro/meso-scale upsetting, J. Mater. Process. Technol. 212 (2012) 640–646.
[28] S.V. Komarov, S.E. Romankov, Mechanical metallization of alumina substrate through shot impact treatment, J. Eur. Ceram. Soc. 34 (2014) 391–399.
[29] M. Meshkat, S. Serajzadeh, A study on non-isothermal static recrystallization during hot rolling of carbon steels, Mater. Manuf. Process. 28 (2013) 236–241.
[30] H. Liang, H. Guo, Y. Ning, X. Peng, C. Qin, Z. Shi, Y. Nan, Dynamic recrystallization behavior of Ti–5Al–5Mo–5V–1Cr–1Fe alloy, Mater. Des. 63 (2014) 798–804.
[31] X.-M. Chen, Y. Lin, M.-S. Chen, H.-B. Li, D.-X. Wen, J.-L. Zhang, M. He, Microstructural evolution of a nickel-based superalloy during hot deformation, Mater. Des. 77 (2015) 41–49.
[32] W.S. Liu, Q. Zhang, Y. Lan, S. Chen, X. Yan, Q. Zhang, H. Wang, D. Wang, G. Chen, Z. Ren, Thermoelectric property studies on Cu-doped n-type $Cu_xBi_2Te_{2.7}Se_{0.3}$ nanocomposites, Adv. Energy Mater. 1 (2011) 577–587.
[33] S.-S. Lin, C.-N. Liao, Effect of ball milling and post treatment on crystal defects and transport properties of $Bi_2(Se,Te)_3$ compounds, J. Appl. Phys. 110 (2011) 093707.
[34] M. Jeong, J.-Y. Tak, S. Lee, W.-S. Seo, H.K. Cho, Y.S. Lim, Effects of Cu incorporation as an acceptor on the thermoelectric transport properties of $Cu_xBi_2Te_{2.7}Se_{0.3}$ compounds, J. Alloy. Compd. 696 (2017) 213–219.
[35] M. Takashiri, S. Tanaka, H. Hagino, K. Miyazaki, Combined effect of nanoscale grain size and porosity on lattice thermal conductivity of bismuth-telluride-based bulk alloys, J. Appl. Phys. 112 (2012) 084315.
[36] C. Dames, G. Chen, Thermal Conductivity of Nanostructured Thermoelectric Materials, CRC Press, Boca Raton, FL, 2006, p. 421.
[37] L. Yang, Z.-G. Chen, M. Hong, G. Han, J. Zou, Enhanced thermoelectric performance of nanostructured Bi_2Te_3 through significant phonon scattering, ACS Appl. Mater. Interfaces 7 (2015) 23694–23699.
[38] X. Yan, B. Poudel, Y. Ma, W. Liu, G. Joshi, H. Wang, Y. Lan, D. Wang, G. Chen, Z. Ren, Experimental studies on anisotropic thermoelectric properties and structures of n-type $Bi_2Te_{2.7}Se_{0.3}$, Nano Lett. 10 (2010) 3373–3378.